



# Novel piezoelectric-based ocean wave energy harvesting from offshore buoys



Seyedeh Fatemeh Nabavi, Anooshiravan Farshidianfar, Aref Afsharfard\*

Mechanical Engineering Department, Ferdowsi University of Mashhad, Mashhad, Iran

## ARTICLE INFO

### Keywords:

Energy harvesting  
Piezoelectric  
Ocean wave  
Buoy

## ABSTRACT

Ocean wave energy is one of the huge energy sources, which easily wasted around us. Because of low frequency of the ocean waves, less attention has been paid on vibration-based energy harvesting from this energy source. In this study, a novel beam-column piezoelectric-based energy harvesting system is studied, which can be optimally used as an Ocean Wave Energy Harvester (OWEH). In doing so, the electromechanical equations of motion for the energy harvesting system are accurately derived. The results, which are obtained using the governing equations, are validated by experimental results. Then application of the presented energy harvesting system, which is installed in offshore buoys, is studied. It is shown that harvested energy is enough to provide needed energy of the electrical devices in the buoy. It is shown that the energy harvesting system in the buoy, which is subjected to large wave height and low frequency, is more efficient. Finally, application of the self-tuning buoy, which works based on the ocean wave frequency, is studied. The presented novel system opens new field of research that helps to use the ocean wave energy in a proper way.

## 1. Introduction

Nowadays, regarding to unlimited demand of energy, many studies are focused on energy harvesting [1,2]. The main aim of these investigations is producing useful energy from sources of energy, which are wasted [3,4]. The ocean wave energy is one of these sources of energy [5–8]. Energy density of the ocean waves is higher than other renewable resources such as solar and wind energy [5]. In case of the deep water ocean waves, average of the energy flux per width of waves is between 40 and 70 KW [5]. The Ocean Wave Energy Harvesting (OWEH) can be divided into three parts: (a) absorber; (b) transducer; and (c) power storage. An absorber collects ocean waves and can be categorized in onshore such as Limpet [9], near shore such as Wavestar [10] and offshore such as Pelamis [11]. The problem with these absorbers is the occupied space, which can negatively effect on environment. Furthermore, it should be noted that the wave energy decreases near coastline and the deep water in offshore is better place for energy harvesting [5].

Because of multifunctional application of buoy, which is originally a navigation device, in this study these systems are chosen as absorber. Between the electromagnetic, piezoelectric and turbine transducers, which have been used in OWEH [5–8], the piezoelectric method is chosen in this study. The energy density of piezoelectric energy harvesting is three times bigger than electromagnetic energy harvesting

[12]. Also, piezoelectric transductions occupy smaller space than turbine transductions.

Historically, Persian windmills (500–900 A.D.) were the first wave energy harvesting systems [13]. Therefore, the wave energy harvesting is one of the human's ancient skills. In past decade, Zurkinden et al. introduced a wave energy harvesting structure, which includes piezoelectric layers with foam core [14]. Murray and Rastegar simulated and studied a piezoelectric OWEH [15]. They discussed about efficiency of converting the ocean wave energy to electrical energy. Orazov et al. studied dynamics of buoy-type energy harvesting system using the mass-spring model [16]. Erturk and Delporte used flexible piezoelectric composites as an energy harvester in underwater system [17]. Cha et al. investigated different geometry of underwater piezoelectric composite beams subjected to base excitation [18]. Xie et al. suggested an energy harvesting system, which focused on longitudinal motions of sea waves [19]. Piezoelectric-based energy harvesting from the transverse ocean waves was studied by Xie et al. [20]. Ionic polymer metal composite was used as transducer in special under water energy harvesting system [21]. Wu et al. presented OWEH with a several piezoelectric coupled cantilever attached to a buoy structure [22]. Viet et al. presented a floating mass-spring energy harvesting system with piezoelectric bar [23]. Hwang et al., in their study, focused on multi-directional systems to harvest energy of ocean waves [24]. Mutsuda et al. studied a novel painted piezoelectric device to use as an ocean energy harvester and

\* Corresponding Author.

E-mail address: [afsharfard@um.ac.ir](mailto:afsharfard@um.ac.ir) (A. Afsharfard).

investigated the relationship between output voltage and parameters of ocean [25].

In the present study, the main idea is present an OWEH, which both of the wave frequency and wave height are considered in its design. Unlike previous studies done on application of large-scale systems, which can work with low frequency, in the present study, a small-scale OWEH is considered. For this reason, a beam-column piezoelectric structure is proposed and a novel theoretical approach for studying behavior of this system is presented. By considering mass ratios, natural frequencies of system can simply be obtained based on parameters of the beam-column. Therefore, a small-scale OWEH, which can work near the frequency of resonance, can be designed. Consequently, the presented OWEH can provide maximum electrical energy. This system can be used in small-scale buoy for generating needed electrical energy of low power consumption sensors. In doing so, system is theoretically modeled and its governing electromechanical equations of motion are experimentally validated. Then regarding to the linear ocean wave assumptions and using the real data of weather stations, application of the presented system is studied.

## 2. Mathematical modeling

Consider a clamped-guided beam-column of length  $L$  and flexural stiffness  $EI$  with tip mass  $M_{tip}$  as shown in Fig. 1. Note that subscripts  $b$  and  $p$  respectively denote beam and piezoelectric. Furthermore,  $\rho$ ,  $t_b$  and  $t_p$  are respectively mass density, beam thickness and piezoelectric thickness. The clamped-guided piezoelectric beam is connected to the moving mass ( $M_{base}$ ), which is exposed to external load  $F$  and  $K$  and  $C$  are stiffness and damping coefficient. Variable  $w$  is the transverse displacement of the beam-column. The displacement of  $M_{base}$  is shown with  $Z$ . Furthermore,  $L$  is length of beam-column.

In the presented study, regarding to the Euler Bernoulli beam theory, the piezoelectric device is modeled as clamped-guided beam with tip mass. Based on the Euler-Bernoulli theory, the equation of the potential energy for the presented system is as follows:

$$\pi = \int_0^L (EI_b + EI_p) \left( \frac{\partial^2 w}{\partial x^2} \right)^2 dx - \int_0^{L_e} z w_p V e_{31} \left( \frac{\partial^2 w}{\partial x^2} \right) dx + \frac{1}{2} K Z^2 \quad (1)$$

where  $V$  and  $L_e$  are electrical voltage and effective length. Furthermore,  $e_{31}$  is effective piezoelectric stress constant. The kinetic energy for the system can be written as follows:

$$T = \int_0^L (\rho_b t_b w_b + \rho_p t_p w_p) \left( \frac{\partial w}{\partial t} + \dot{Z} \right)^2 dx + \frac{1}{2} M_{base} \dot{Z}^2 + \frac{1}{2} M_{tip} \left( \dot{Z} + \frac{\partial w}{\partial t} \Big|_{x=L} \right)^2 \quad (2)$$

where  $w_b$  and  $w_p$  are respectively the beam and piezoelectric width.

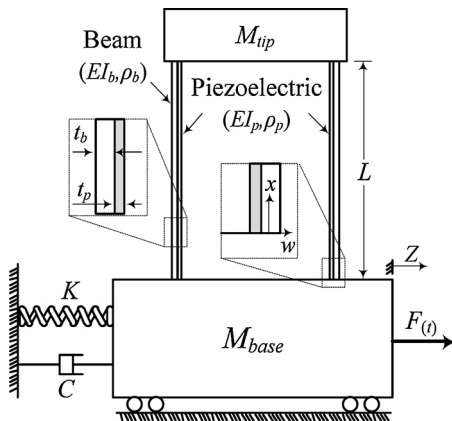


Fig. 1. Schematic of the clamped-guided piezoelectric beam with tip mass.

The internal electrical energy in the presented system can be given by:

$$W_{ie} = - \int_0^{L_e} z w_p e_{31} V \frac{\partial^2 w}{\partial x^2} dx - \int_0^L w_p e_{33} V^2 / t_p dx \quad (3)$$

where  $e_{33}$  is permittivity component at constant strain and the piezoelectric layer width. Furthermore,  $z$  is distance from neutral axis. The non-conservative virtual work of the system is written as follows:

$$\delta W_e = F \delta Z + N \int_0^L \frac{\partial w}{\partial x} \delta \left( \frac{\partial w}{\partial x} \right) dx - Q \delta V - C \dot{Z} \delta Z - f_d \delta q_i \quad (4)$$

where  $N$  is the axial load and in this study it is equal to  $M_{tip}g$  and  $F$  is the external load [26]. Furthermore,  $Q$  is the electric charge and  $f_d$  is the damping force. Using the separation of variable method, displacement of the beam can be given as follows:

$$w(x, t) = \sum_{i=1}^n \varphi_i(x) q_i(t) \quad (5)$$

where  $\varphi(x)$  and  $q(t)$  indicate mode shape and the time response. The electromechanical Lagrange equations can be expressed as [27]:

$$\frac{d}{dt} \left( \frac{\partial T}{\partial \dot{q}_i} \right) - \frac{\partial T}{\partial q_i} + \frac{\partial \pi}{\partial q_i} - \frac{\partial W_{ie}}{\partial q_i} = N q_i \int_0^L \left( \frac{d\varphi}{dx} \right)^2 dx - f_d \quad (6)$$

$$\frac{d}{dt} \left( \frac{\partial T}{\partial \dot{Z}} \right) - \frac{\partial T}{\partial Z} + \frac{\partial \pi}{\partial Z} - \frac{\partial W_{ie}}{\partial Z} = F - C \dot{Z} \quad (7)$$

$$\frac{d}{dt} \left( \frac{\partial T}{\partial \dot{V}} \right) - \frac{\partial T}{\partial V} + \frac{\partial \pi}{\partial V} - \frac{\partial W_{ie}}{\partial V} = Q \quad (8)$$

Substituting Eq (5) into Eqs (1–3) and regarding to the Lagrange equations, the following relations will be obtained:

$$m_{eq} \ddot{q}_i + c_{eq} \dot{q}_i + (k_{eq} - k_g) q_i - \theta V = -m^* \dot{Z} \quad (9)$$

$$M_{eq} \ddot{Z} + C \dot{Z} + K Z = F - m^* \ddot{q} \quad (10)$$

$$C_p \dot{V} + V/R + \theta \dot{q}_i = 0 \quad (11)$$

where the coefficients of the above equations and the capacitance of piezoelectric layer  $C_p$  are expressed as:

$$m_{eq} = 2 \int_0^L (\rho_b t_b w_b + \rho_p t_p w_p) \varphi^2 dx + M_{tip} \varphi^2(L) \quad (12)$$

$$m^* = 2 \int_0^L (\rho_b t_b w_b + \rho_p t_p w_p) \varphi dx + M_{tip} \varphi(L) \quad (13)$$

$$k_{eq} = 2 \int_0^L (EI_b + EI_p) \left( \frac{d^2 \varphi}{dx^2} \right)^2 dx \quad (14)$$

$$k_g = N \int_0^L \left( \frac{d\varphi}{dx} \right)^2 dx \quad (15)$$

$$c_{eq} = 2\zeta \sqrt{k_{eq} m_{eq}} \quad (16)$$

$$\theta = 2 \int_0^{L_e} z w_p e_{31} \left( \frac{d^2 \varphi}{dx^2} \right) dx \quad (17)$$

$$M_{eq} = 2(\rho_b t_b w_b + \rho_p t_p w_p) L + M_{tip} + M_{base} \quad (18)$$

$$C_p = 2 \int_0^L w_p e_{33} / t_p dx \quad (19)$$

In the above equations,  $\zeta$  is the damping. Regarding to the Euler-Bernoulli theory, the mode shape of vibration for the system can be written as follows:

$$\varphi_i(x) = C_i \{ \cos(\lambda_i x/L) - \cosh(\lambda_i x/L) + \sigma_i (\sin(\lambda_i x/L) - \sinh(\lambda_i x/L)) \} \quad (20)$$

where  $\lambda_i$  is the eigenvalue of the  $i$ th vibration mode, which can be obtained using the characteristic equation. This equation is derived regarding to the eigenfunction and the boundary conditions. The

**Table 1**  
Values of the eigenvalue and equivalent mass and stiffness in the first mode of vibration.

$M_{tip}/m_{bp}$	0.00	0.20	0.40	0.60	0.80	1.00	5.00	10.00	50.00	100.00
$\lambda_1$	2.3651	2.1334	1.9823	1.8726	1.7876	1.7189	1.2226	1.0371	0.6987	0.5881
$\sigma_1$	-0.9825	-1.0403	-1.0925	-1.1390	-1.1808	-1.2188	-1.6562	-1.9408	-2.8666	-3.4037
$k_{eq}L^3/EI_{bp}$	24.8080	24.3408	24.1908	24.1230	24.0818	24.0598	24.0164	24.0150	24.0186	24.0258
$k_gL/N$	1.2194	1.2107	1.2071	1.2053	1.2041	1.2034	1.2009	1.2003	1.2003	1.2003
$(m_{eq}-M_{tip})/m_{bp}$	0.7930	0.7750	0.7664	0.7616	0.7582	0.7560	0.7462	0.7446	0.7434	0.7432
$(m^*-M_{tip})/m_{bp}$	1.0464	1.0300	1.0222	1.0176	1.0144	1.0124	1.0032	1.0018	1.0004	1.0004

characteristic equation can be obtained as follows:

$$1 - \cos(\lambda_i) \cosh(\lambda_i) - \frac{\rho AL}{\lambda_i M_{tip}} (\cos(\lambda_i) \sinh(\lambda_i) + \cosh(\lambda_i) \sin(\lambda_i)) = 0 \tag{21}$$

Note that  $\omega_i$  is the undamped natural frequency of the  $i$ th vibration mode ( $\omega^2 = EI\lambda^4 / (\rho AL)$ ) and  $\sigma_i$  is a coefficient which can be calculated using the following relation:

$$\sigma_i = \frac{(\sin(\lambda_i) - \sinh(\lambda_i)) + \frac{M_{tip}\lambda_i}{\rho AL} (\cos(\lambda_i) - \cosh(\lambda_i))}{(\cos(\lambda_i) + \cosh(\lambda_i)) - \frac{M_{tip}\lambda_i}{\rho AL} (\sin(\lambda_i) - \sinh(\lambda_i))} \tag{22}$$

The equivalent mass and stiffness of system can be obtained by substituting Eq (20) into Eqs. (12–15). These values, for several mass ratios, are presented in Table 1. Note that  $m_{bp}$  and  $EI_{bp}$  are respectively the mass and flexural stiffness of the piezoelectric beam and they are equal to  $m_{bp} = (\rho_b t_b w_b + \rho_p t_p w_p)L$  and  $EI_{bp} = E_b I_b + E_p I_p$ .

The fundamental frequency of the system can be obtained by  $\omega^2 = (k_{eq} - k_g) / m_{eq}$ . Note that the natural frequency of the mechanical systems is related to stiffness over mass ( $k/m$ ) and gravitational constant over length ( $g/L$ ). Therefore, in the present study, fundamental frequency can simply be written as  $\omega^2 = \alpha (EI_{bp} / L^3 m_{bp}) - \beta (g/L)$ . For several mass ratios coefficients  $\alpha$  and  $\beta$  are presented in Table 2. Note that, in first columns of Table 1 and Table 2, the tip mass is considered to be equal to zero to compare the results with previously presented result [28]. Generally, in the case of energy harvesting systems, like the system presented in this study, the tip mass is not equal to zero.

Variation of the non-dimensional frequency ( $\omega^2 m_{bp} L^3 / EI_{bp}$ ) versus mass ratio ( $M_{tip} / m_{bp}$ ) and inverse of non-dimensional flexural stiffness ( $m_{bp} g L^2 / EI_{bp}$ ) is shown in Fig. 2.

The approximated polynomial function, which is obtained using the surface fitting toolbox in MATLAB software, for finding the fundamental frequency of the system with respect to the length of beam-column, mass, flexural stiffness and tip mass is given as follows:

$$\frac{\omega^2 m_{bp} L^3}{EI_{bp}} = \begin{cases} 31.39 - 31.91 \frac{M_{tip}}{m_{bp}} - 0.42 \frac{m_{bp} g L^2}{EI_{bp}} & ; 0 < \frac{M_{tip}}{m_{bp}} < 1 \\ + 14.22 \left(\frac{M_{tip}}{m_{bp}}\right)^2 & \\ 17.62 - 3.85 \frac{M_{tip}}{m_{bp}} - 0.42 \frac{m_{bp} g L^2}{EI_{bp}} & ; 1 < \frac{M_{tip}}{m_{bp}} < 10 \\ + 0.23 \left(\frac{M_{tip}}{m_{bp}}\right)^2 & \\ 2.013 - 0.02 \frac{M_{tip}}{m_{bp}} + 0.13 \frac{m_{bp} g L^2}{EI_{bp}} & ; 10 < \frac{M_{tip}}{m_{bp}} < 100 \\ - 0.07 \left(\frac{m_{bp} g L^2}{EI_{bp}}\right)^2 & \end{cases} \tag{23}$$

**Table 2**  
Values of the eigenvalue and equivalent mass and stiffness in the first mode of vibration.

$M_{tip}/m_{bp}$	0.00	0.20	0.40	0.60	0.80	1.00	5.00	10.00	50.00	100.00
$k_gL/m_{bp}g$	0	0.2421	0.4843	0.7232	0.9633	1.2034	6.0170	12.0030	60.0150	120.03
$m_{eq}/m_{bp}$	0.7930	0.9750	1.1664	1.3616	1.5582	1.7560	5.7560	10.7446	50.7434	100.7432
$\alpha$	31.2894	20.9649	20.7397	17.7167	15.4549	13.7015	4.1724	2.2351	0.4733	0.2385
$\beta$	0	0.2483	0.4152	0.5311	0.6182	0.6853	1.0453	1.1171	1.1827	1.1914

The above equation can be used to find an accurate approximation for the natural frequency of the presented system based on the mass ratio and the non-dimensional frequency. It is desirable to have a system work near the fundamental frequency of system. Therefore, only first mode of vibration, which leads to have large deflection, is considered. To accurately find the first mode shape of vibration for the discussed beam-column, the wave equation, based on the Euler-Bernoulli assumption, is considered as follows [29]:

$$EI \frac{\partial^4 w}{\partial x^4} + \rho A \frac{\partial^2 w}{\partial t^2} - M_{tip} g \frac{\partial^2 w}{\partial x^2} = 0 \tag{24}$$

In the above equation  $w(x,t) = \varphi(x)q(t)$  where  $\varphi(x) = e^{sx}$  and  $q(t) = \sin(\omega t)$ . Substituting  $w(x,t)$  into the wave equation, leads to find the characteristic equation as follows:

$$s^4 - (M_{tip}g/EI)s^2 - (\rho A/EI)\omega^2 = 0 \tag{25}$$

Roots of the characteristic equation can be given by:

$$s_1^2, s_2^2 = \frac{M_{tip}g}{2EI} \pm \left( \frac{M_{tip}^2 g^2}{4E^2 I^2} + \frac{\rho A \omega^2}{EI} \right)^{1/2} \tag{26}$$

Considering boundary conditions, the updated first mode shape of vibration can be obtained in the following form:

$$\varphi'(x) = C' [\cosh(s_1 x) - \cos(s_2 x) + \sigma' \{ \sinh(s_1 x) - (s_1/s_2) \sin(s_2 x) \}] \tag{27}$$

where the coefficient  $\sigma'$  can be calculated using the following relation:

$$\sigma' = \{s_1 \sinh(s_1 L) + s_2 \sin(s_2 L)\} / \{-s_1 \cosh(s_1 L) + s_1 \cos(s_2 L)\} \tag{28}$$

Substituting the updated mode shape of vibration into Eqs. (12–17), leads to find accurate coefficients of the electromechanical governing equations of motion (Eqs. 9–11). In this section, vibratory behavior of a beam-column piezoelectric structure is studied using a novel theoretical approach. Regarding to mass ratios, tabulated data are presented to find natural frequencies of system based on length, flexural stiffness and tip mass. In next section, the theoretical result, which are obtained in this section, is validated by experiment.

### 3. Experimental study

To validate the developed equation of motion for the discussed system, a prototype is fabricated and tested. As shown in Fig. 3, presented system is attached to MS-100N shaker that provides the base excitation. The LA200 power amplifier provides power in the form of voltage and current to the shaker. An IEPe accelerometer (GT-AU02) is positioned at the tip of the piezoelectric beam-column and the impedance head is attached to the base (main mass), which measures the force and acceleration of the main mass. Sampling frequency of the

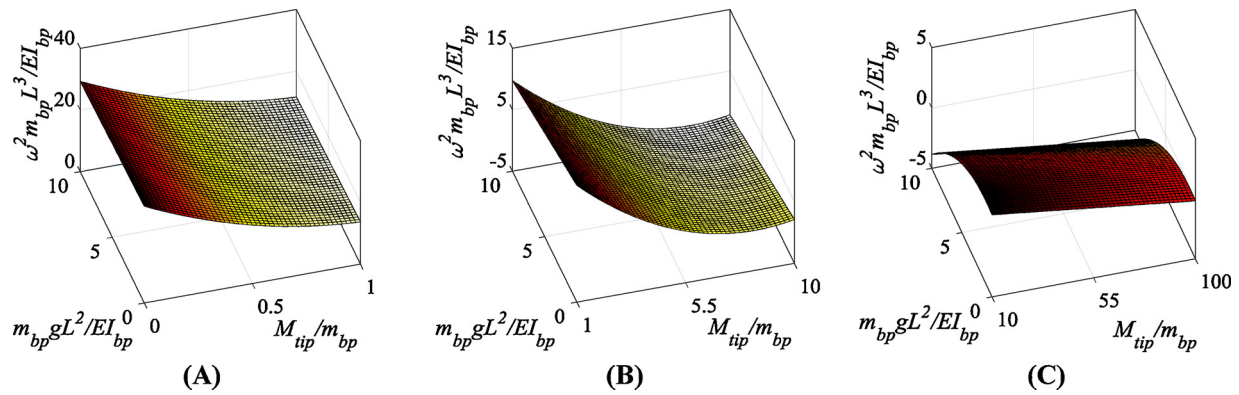


Fig. 2. Variation of the non-dimensional frequency with the mass ratio and  $m_{bp}gL^2/EI_{bp}$  for  $0 < M_{tip}/m_{bp} < 1$  (A);  $1 < M_{tip}/m_{bp} < 10$  (B); and  $10 < M_{tip}/m_{bp} < 100$ .

acquisition system is considered to be 10 KHz. Properties of the piezoelectric beam-column, main mass and tip mass are listed in Table 3. Furthermore, properties of the piezoelectric material (PZT), which are used in this study, are presented in the Appendix part.

For two different tip masses ( $M_{tip} = 88.85\text{gr}$  and  $M_{tip} = 108.85\text{gr}$ ), frequency response of the piezoelectric beam-column system, which shows the ratio of the tip mass acceleration with respect to the input force ( $\ddot{q}_{(L)}/F$ ), is shown in part (A) of Fig. 5. Note that the axial force should be enough big to have a system with low fundamental frequency, which doesn't buckle. Part (B) of this figure, shows the amplitude between theoretical and the experimental result, which can be observed in Fig. 4, guarantees accuracy of the presented electro-mechanical modeling. The damping ratio for the clamped-guided piezoelectric beam is experimentally obtained to be equal to 0.0368. In doing so, the damping ratio in the theoretical model is changed to find a frequency response near to the experimental result, which is shown in part (A) of Fig. 4.

#### 4. Case study: beam-column piezoelectric-based buoy

##### 4.1. Ocean waves equations

The ocean waves can be presented by linear, nonlinear and random

Table 3

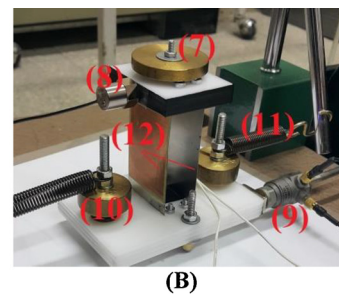
Properties of the presented piezoelectric device.

Parameters	Values	Parameters	Values	Parameters	Values
$E_{B1}$ (GPa)	170.00	$E_{P1}$ (GPa)	62.50	$M_{base}$ (gr)	252.67
$\rho_{B1}$ ( $\text{kg}/\text{m}^3$ )	8500.00	$\rho_{P1}$ ( $\text{kg}/\text{m}^3$ )	7500.00	$K$ (N/m)	$2 \times 2116.60$
$L_{B1}$ (mm)	61.00	$L_{P1}$ (mm)	61.00	$d_{31}$ (pC/N)	-280.00
$t_{B1}$ (mm)	0.15	$t_{P1}$ (mm)	0.11	$e_{33}$ (nC/m)	6.50
$w_{B1}$ (mm)	37.00	$w_{P1}$ (mm)	36.00	$R$ (M $\Omega$ )	10.00

theories. In the present study, the wave steepness, which is the wave height over its length, is considered small. For this reason, the linear or Airy wave theory is considered to describe the sea waves [30]. This theory uses the solution of the linear equation of continuity. According to this theory, the flow under the free surface is assumed to be non-rotational. Regarding to the kinematic and dynamic conditions of free-surface and the sea-floor are considered the wave equation can be derived. The displacement motion of particle caused by the wave is given by [30]:

$$Y = \frac{H}{2} (\sinh [k(z_0 + h)] / \sinh (kh)) \cos(\omega t) \tag{29}$$

where  $H, \omega, k, h$  and  $z_0$  are respectively wave height, wave frequency, wave number, sea depth and position of particle. It should be noted that the wave number is equal to  $k = 2\pi/\lambda$ , in which  $\lambda$  is the wave length. To find the wave frequency, at the first step, the shallow, intermediate or



- 1- Data acquisition system
- 2- Signal generator
- 3- Power amplifier
- 4- Frequency response analyzer
- 5- Oscilloscope
- 6- Shaker
- 7- Tip mass
- 8- Accelerometer
- 9- Impedance head
- 10- Main mass
- 11- Main mass spring
- 12- piezoelectric beams

Fig. 3. Experimental setup for finding the frequency response (A); and the energy harvester (B).

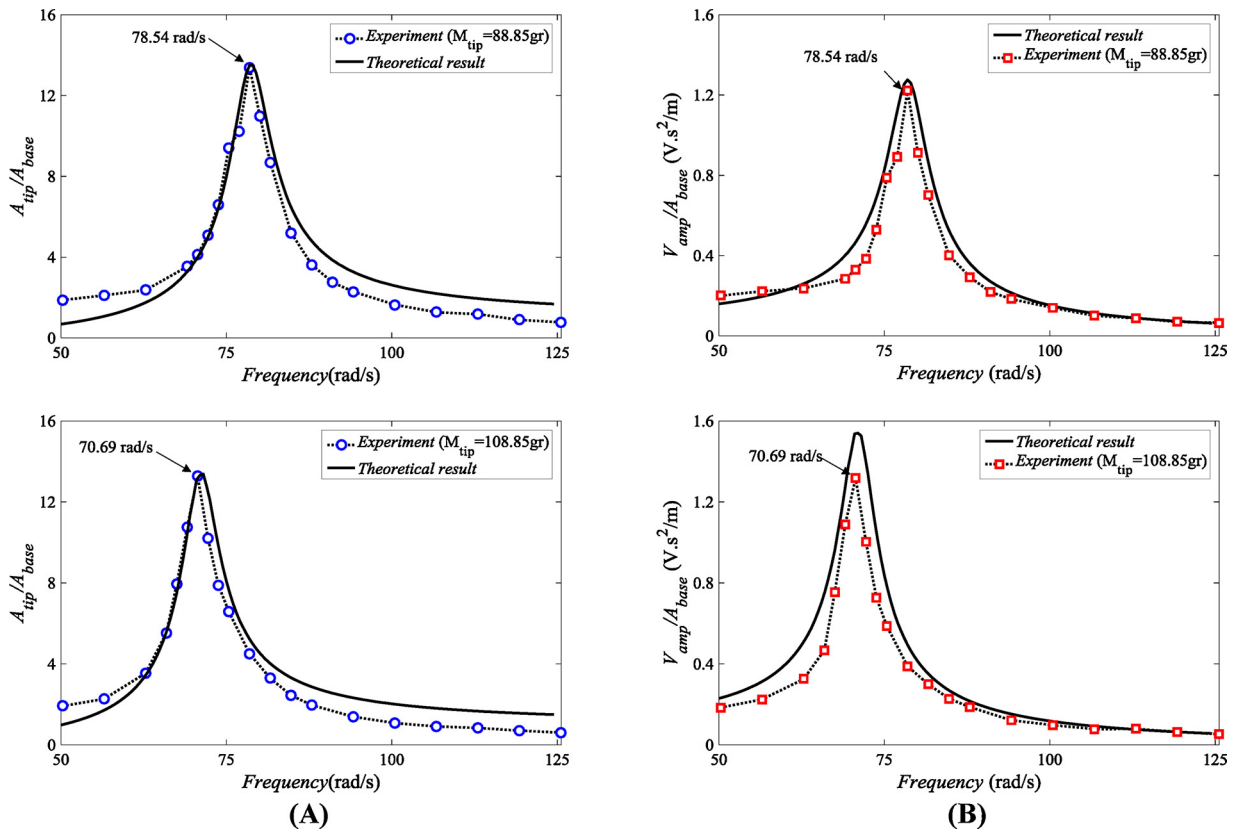


Fig. 4. Frequency response (A); and voltage ratio of each piezoelectric device (B) for two variable tip masses.

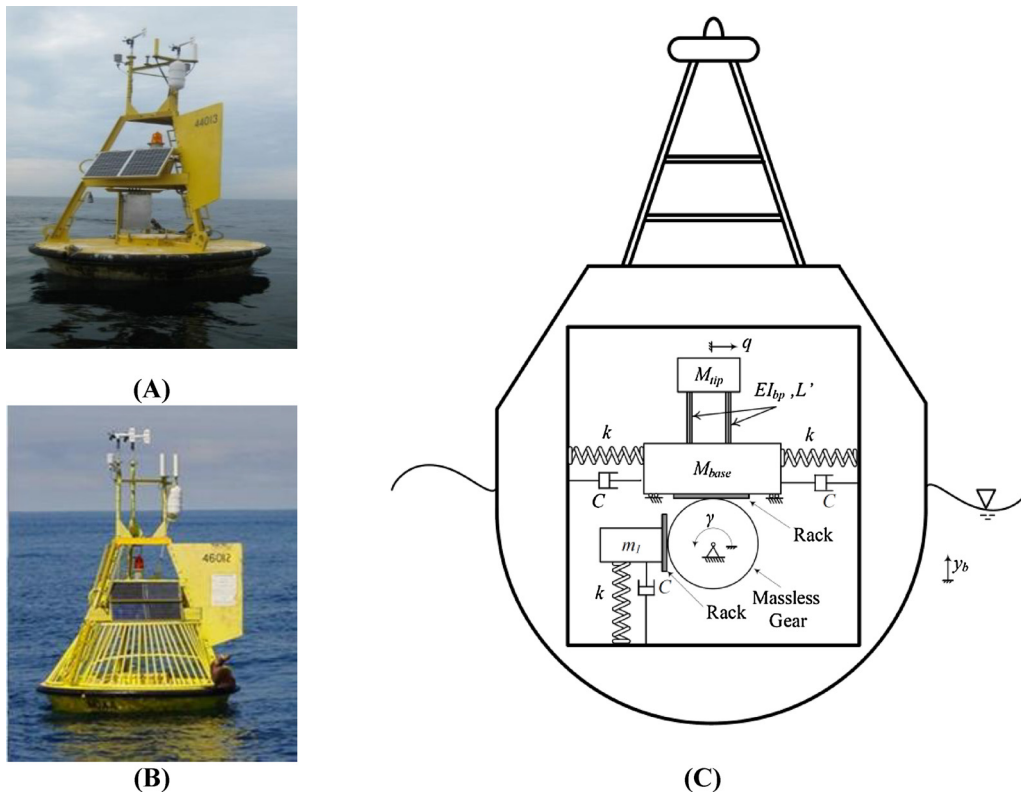


Fig. 5. Buoy BF NOAA station 44,013, Boston 16 NM East of Boston (A) [35]; Half moon bay station 46,012, San Francisco 24 NM SSW of San Francisco (B) [35]; and schematic of a beam-column piezoelectric-based buoy (C).

deep water assumptions should be determined. In the deep water assumption, which is used in this study, the depth is larger than half of the wave length [30]. According to this consideration, the wave frequency can be given by  $\omega_0 = (gk)^{1/2}$ . It should be noted that at a depth of approximately one-half wavelength, the wave effect can be considered to be negligible [31].

#### 4.2. The buoy

The buoy is an aerologic device, which can measure the sea wave properties by chasing the motion of the water particles at the sea surface. Part (A) and part (B) of Fig. 5 show two aerologic buoys in Atlantic and Pacific oceans. Generally, a floating body has six degrees of freedom (surge, sway, heave, roll, pitch and yaw) [32]. Based on previous studies done in power absorption area, buoy is assumed to be restricted to heave motion only. Experimental validations confirm this consideration is correct [33,34]. As shown in this figure, renewable energy source (solar energy) is used to generate needed energy of the buoy electrical devices. In this study, the vibration-based energy sources are used to provide the needed energy. In part (C) of this figure, schematic of the new designed buoy is shown.

Regarding to the energy harvesting mechanism, shown in part (C) of Fig. 5, vertical movement of the buoy ( $y_b$ ), leads to vertical oscillations of  $m_1$ . Note that, in this study, the vertical movement of the buoy ( $y_b$ ) is considered equal to the displacement motion of particle caused by the wave ( $y_b = Y$ ), which is presented in Eq. (29). Then the mass-less gear transmits the motion of  $m_1$  to the base mass ( $M_{base}$ ). It can easily be concluded that the displacement amplitude both  $m_1$  and  $M_{base}$  are the same. Therefore, the electromechanical equations of motion for the presented energy harvesting system can be obtained as follows:

$$m_{eq} \ddot{q}_i + c_{eq} \dot{q}_i + (k_{eq} - k_g) q_i - \theta V = -m^* r \ddot{\gamma} \quad (30)$$

$$\bar{J} \ddot{\gamma} + \bar{c} \dot{\gamma} + \bar{k} \gamma = -m^* r \ddot{q} + Cr \dot{y}_b + Kr y_b \quad (31)$$

$$C_p \dot{V} + V/R + \theta \dot{q}_i = 0 \quad (32)$$

where  $\bar{J} = (M_{eq} + m_1)r^2$ ,  $\bar{c} = 3Cr^2$  and  $\bar{k} = 3Kr^2$  and other coefficients are previously presented in section 2. In the presented model, base excitation of the system is occurred due to the heave motion of ocean. To increase the harvested power, parameter K is selected in a way that natural frequencies of the system be approach to the first and second midyear ocean frequencies. Then C is obtained using the Rayleigh damping method [26]. At here the damping ratio is considered to be equal to 0.01. The monthly average of the wave height and frequency of two different NDBC<sup>1</sup> registered buoys are respectively shown in part (A) and part (B) of Fig. 6. In part (C) of Fig. 6, the wave rate, which is equal to the wave height multiply by the wave frequency, is shown. It should be noted that, the electric power, which can be harvested from the piezoelectric device, depends on strain in the piezoelectric beam-column and its vibration frequency. For simplicity, strain multiplied by frequency is named as "rate of strain" and it depends on the deflection of the piezoelectric beams and its frequency. In the present study, the energy harvesting system is designed to work close to the first natural frequency and only one mode is considered. Therefore, it can be concluded deflection of the piezoelectric beams depends on the ocean wave force amplitude (base excitation), which is related to the wave height. Therefore, it can be concluded that the rate of strain for the piezoelectric beams is related to, the so-called wave rate. Regarding to Fig. 6, average of wave height for stations 44,013 and 46,012 are respectively equal to 0.9863 m, 2.4202 m. Furthermore, averages of the wave frequency for these buoys are respectively equal to 0.8074 rad/s and 1.2937 rad/s.

Note that the discussed buoys are located at fixed points with 64.5 m (for station44013) and 208.8 m (for station46012) depth and average of the depth ratio (depth of ocean over wavelength) for stations

44,013 and 46,012 are respectively equal to 0.6991 and 5.4481, which are higher than 0.5 and consequently, the deep-water assumption is correct [30]. In part (D) of Fig. 6, the wave steepness (wave height over wavelength) is shown. It can be observed that the wave steepness is smaller than 0.5 and the linear wave theory is correct [30]. Regarding to the linear wave theory and deep-water assumption it can be considered the heave motion is the main motion of the buoys, which are investigated in this study [33,34].

It should be noted that the piezoelectric device, which its response is shown in Fig. 4, is a part of the energy harvesting system that is connected to another mass-spring system ( $m_1, k$ ). Therefore, by changing  $k$  or  $m_1$  the natural frequencies of the system can be tuned to be near to the ocean wave frequency.

## 5. Results and discussion

### 5.1. Conventional energy harvesting buoy

Regarding to the parameters of ocean wave and the electro-mechanical equations of motion, the output power is studied in this section. Note that the energy harvesting system, which is used in the buoy, is a two degree of freedom system. In order to harvest maximum energy, the frequencies of the system should be near to the ocean frequency. By dividing a year into first and second midyears, two ocean wave frequencies are considered to adapt OWEH with the ocean waves along a year. The Perfection Rate (P.R.), which shows vicinity of the energy harvesting system natural frequencies and the ocean wave frequencies, is introduced as:

$$P. R. = \left( 1 - \frac{(\omega_{2H} - \omega_{2ndocean}) + (\omega_{1H} - \omega_{1stoccean})}{(\omega_{1stoccean} + \omega_{2ndocean})/2} \right) \times 100 \quad (33)$$

where  $\omega_{1H}$  and  $\omega_{2H}$  are respectively first and second natural frequencies of OWEH. Furthermore,  $\omega_{1th\ ocean}$  and  $\omega_{2nd\ ocean}$  are respectively the first and second midyear frequencies. Regarding to the perfection rate, parameters of the synchronized energy harvesting system are equal  $L = 91.50$  mm,  $M_{base} = 32$ kg and  $m_1 = 16$ kg. It should be noted that, other parameters of the system, which are related to the piezoelectric material and dimension of the piezoelectric beam are considered constant. Furthermore, because of different frequencies of the ocean waves, the tip mass for stations 44,013 and 46,012 are respectively equal to 688.80gr and 695.50gr. Effect of changing the stiffness K on both frequencies and the perfection rate is shown in Fig. 7. According to this figure, it can be concluded that the best stiffness K is where the P.R. parameter is maximum. This figure illustrates that increasing the stiffness leads to increase the frequencies of both systems. As shown in part (A) of Fig. 7, for station 44,013, highest P.R. occurs when  $K = 27.5$  N/m. Part (B) of this figure, shows that in station 46,012, maximum P.R. happens if  $K = 10.0$  N/m. Parts (C) and (D) of Fig. 7, show the frequency responses of the system, which are tuned to work in stations 44,013 and 46,012, respectively.

Like the mechanical changes, which increase the P.R. parameter, changing the electrical load resistance can result in increasing the harvested electrical power. Effect of changing the load resistance on the root mean square of the output power ( $P_{rms}$ ) is shown in parts (A) and (B) of Fig. 8. In this figure, the time response of the non-dimensional output voltage ( $V/V_{max}$ ) is shown for  $R = 500$  K $\Omega$  and  $R = 7.5$  M $\Omega$ . As illustrated in part (A) of this figure, for station 44,013, increasing the load resistance up to 4.0 M $\Omega$  in first midyear and 3.5M $\Omega$  in second midyear leads to increase the output harvested power. Based on part (B) of this figure, the maximum power generation by the station 46,012 can be observed for the load resistances 6.5 M $\Omega$  and 7.0 M $\Omega$  in first and second midyears. Furthermore, regarding to Fig. 8, it can be concluded that the power generation of both stations in first midyear is bigger than the second midyear. It is reasonable, because the mean of wave height in first midyear is bigger than second midyear. Regarding to Fig. 8, it

<sup>1</sup> National Data Buoy Center.

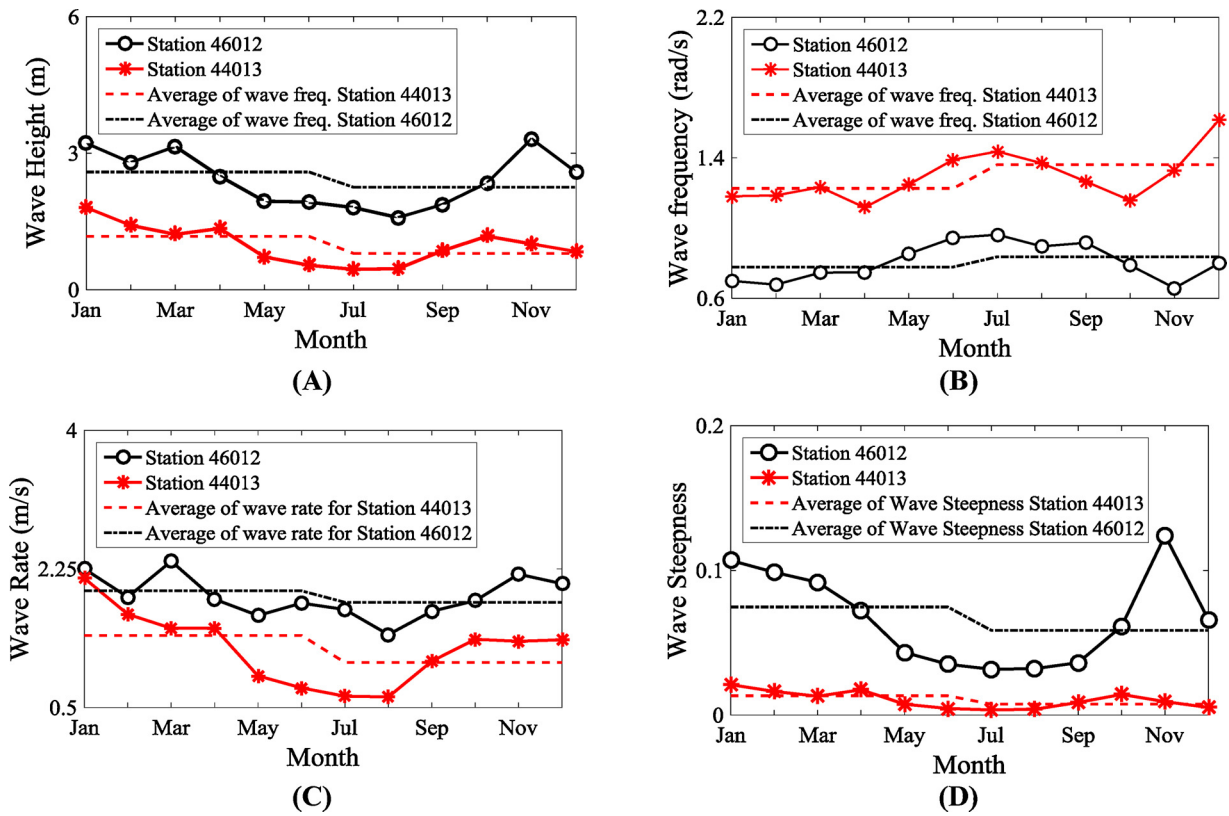


Fig. 6. The wave height (A); wave frequency (B); wave rate (C); and wave steepness (D) for different months in 2016 for station 46,012 and 44,013[35].

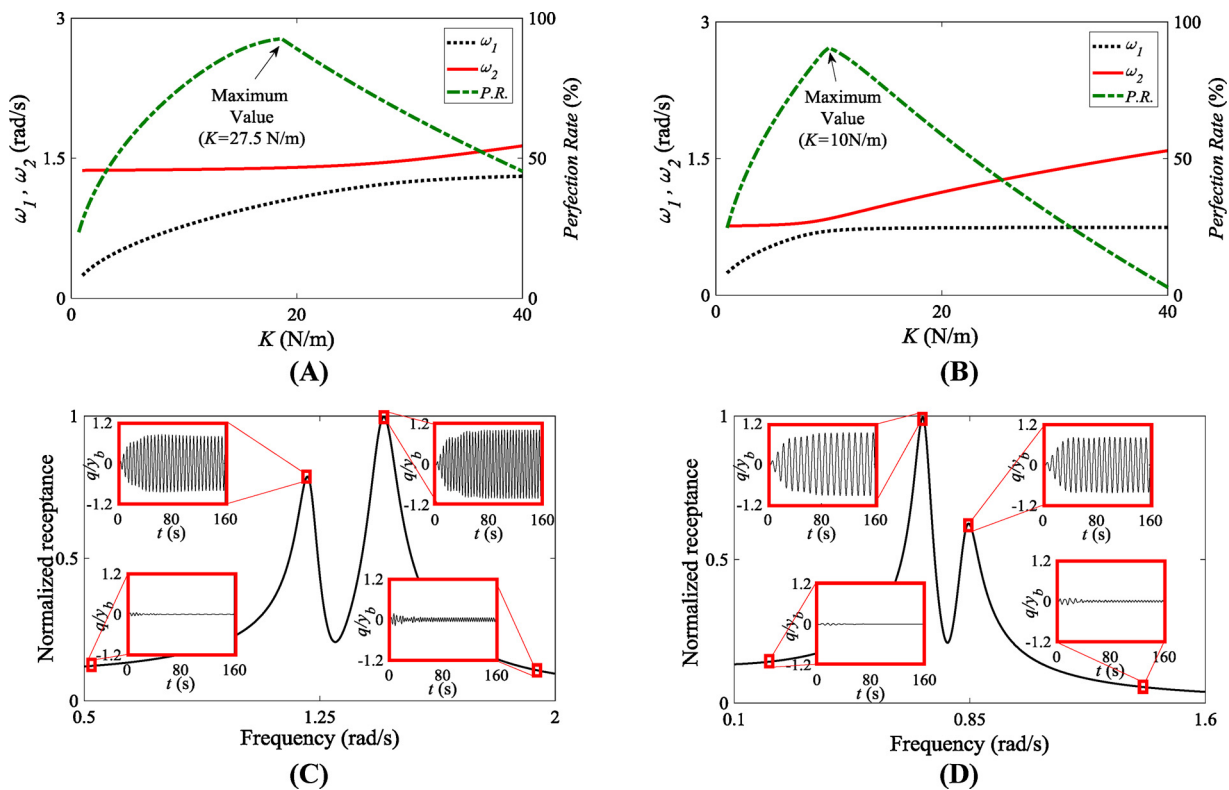


Fig. 7. Effect of changing the stiffness on first and second frequencies and Perfection Rate (P.R.) in station 44,013 (Boston) (A); and station 46,012 (San Francisco) (B) frequency response the system located in Boston (C) and San Francisco (D).

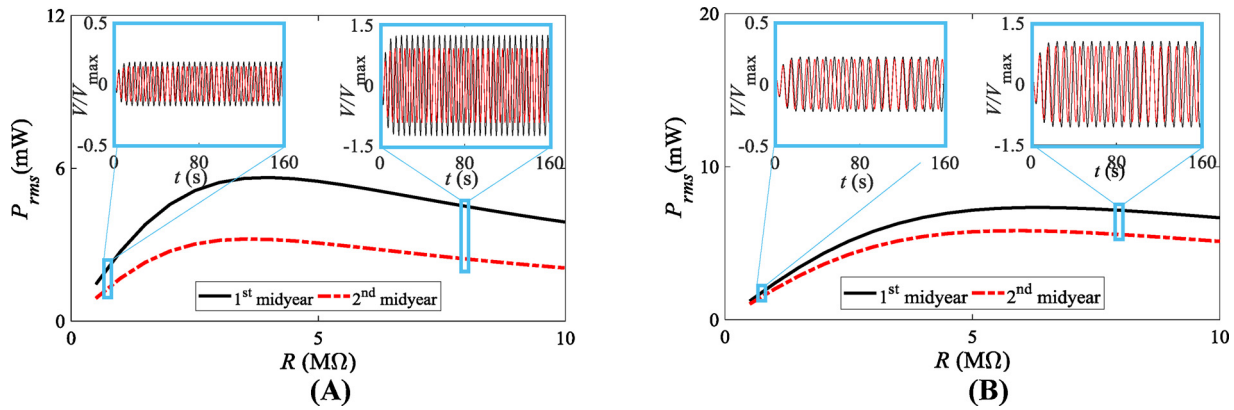


Fig. 8. Effect of changing the load resistance on the output power for first and second midyear in station 44,013 (Boston) (A); and station 46,012 (San Francisco) (B).

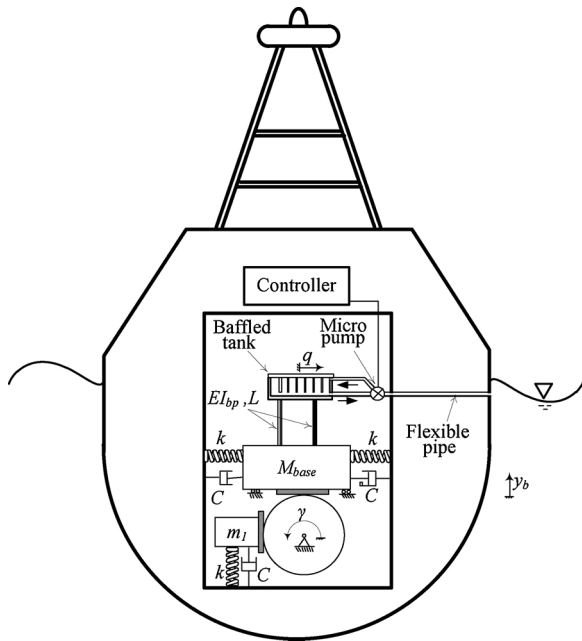


Fig. 9. Schematic of the self-tuning buoy.

can be concluded that the station located at the San Francisco offshore can generate more power than the system in Boston offshore. So San Francisco because of larger height waves is better option for OWEH.

Regarding to inaccessibility of offshore buoys, the needed energy of electrical parts, which are used in these systems, should independently be generated inside the buoys.

Table 4

The power consumption of different sensors of buoy.

Sensor name (model)	Voltage (V)	Power (mW)	Reference
Wave Height (3595)	7-14	24-98	[37]
Analog Pressure (Rev-11-1107-DS)	0.5-5	5-50	[38]
Turbidity (DTS-12)	9.6-16	3.36-5.6	[39]
Turbidity (4112)	7-20	24.5-70	[37]
Turbidity and temperature (Ponsel SE00017)	5-12	21-50.4	[40]
Temperature (S-5851A Series)	2.7	1.22	[41]
Wind Speed & Direction (Windsonic)	12	24	[42]

### 5.2. Self-tuning buoy

In the Self-tuning buoy, the tip mass is replaced with a baffled water tank. Therefore, the tip mass can be controlled with changing the volume of the ocean water in the baffled tank. For this reason, regarding to the wave frequency, which is measured by the sensors installed in the buoy, volume of the water in the tank is changed to tune the first natural frequency of the system with the ocean wave frequency. Fig. 9 shows the schematic of the discussed smart beam-column piezoelectric-based buoy.

Herein, for example, application of the self-tuning buoy in station 44,013 (Boston) is studied. Variation of the first natural frequency of system versus the tip mass is shown in part (A) of Fig. 10. As shown in this figure, changing the tip mass between 500 g and 1.2 kg results in the natural frequency varies between 0.87 rad/s and 1.73 rad/s. In part (A) of Fig. 10, a curve is fitted to theoretically obtained natural frequencies. To increase the output voltage, the mass ratio should be change in a way that the system works close to its natural frequency. Therefore, the mass ratio in the self-tuning buoy should vary to synchronize the natural frequency of system with the ocean wave frequency. The tip mass should change with

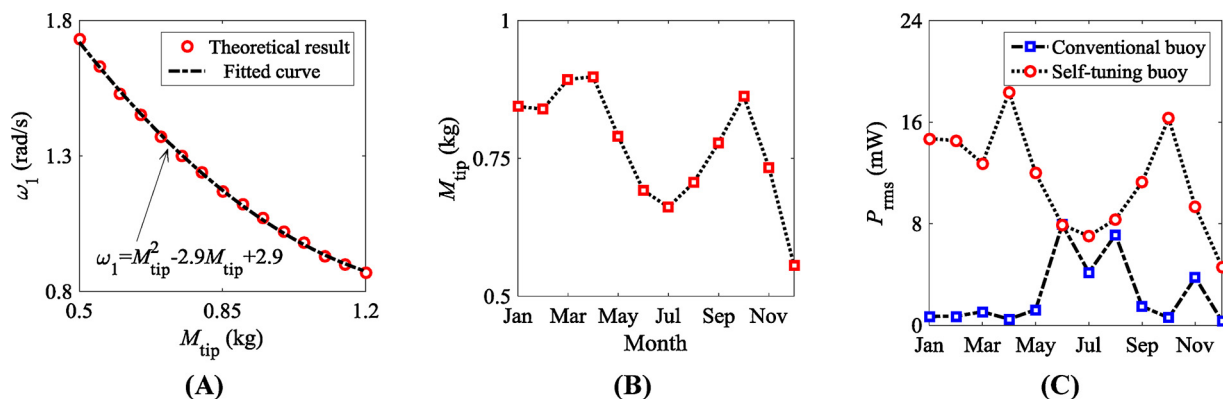


Fig. 10. Variation of the fundamental frequencies versus the tip mass (A); needed tip mass during a year (B); and harvested power during a year.

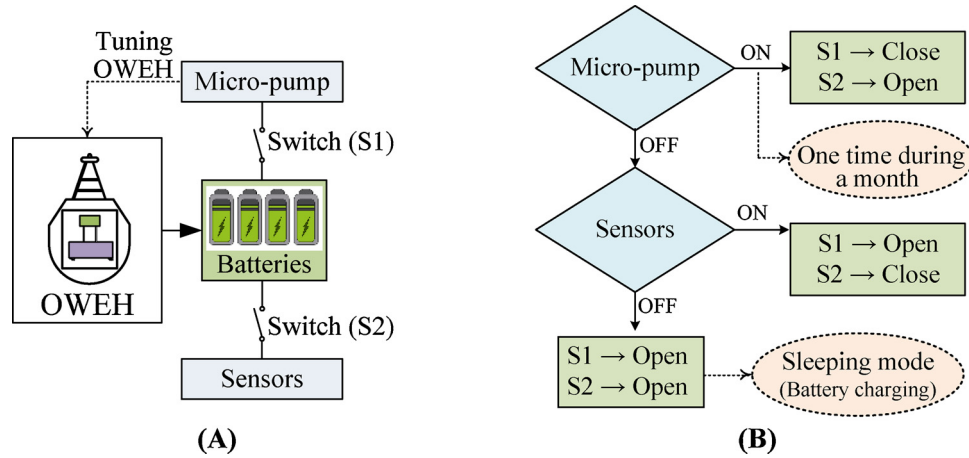


Fig. 11. Simple schematic of the electrical parts in the Self-tuning buoy (A); and function (ON/OFF) of switches during application of the self-tuning buoy (B).

respect to the pattern, which is shown in part (B) of Fig. 10. This pattern is obtained using the ocean wave frequency, which is presented in part (B) of Fig. 6. In part (C) of Fig. 10, root mean square of the harvested power, using the self-tuning buoy during a year is compared with the output power from the conventional buoy. As shown in this figure, in the self-tuning buoy the output power effectively increased with respect to the conventional buoy.

Some of sensors, which are used in the offshore buoys, are provided in Table 4. As shown in this table, power consumption of these sensors is smaller than 100 mW. Note that in the presented system, several OWEH's, which are small devices, can be used to generate enough energy for the sensors. Furthermore, it should be mentioned that all of the sensors don't work all time. During the sleep mode of sensors, the harvested energy can be saved in batteries. Schematic of the electrical parts of the self-tuning buoy is simply shown in part (A) of Fig. 11. Function of S1 and S2 switches, which are shown in this figure, is explained in part (B) of Fig. 11. It should be noted that tip-mass in the self-tuning buoy should be changed one time in a month. Therefore, the micro pump should only work one time in a month. Needed energy of the micro-pumps can be supplied by batteries, which can charge by several OWEH's that work during month. Moreover, the energy consumption of a usual micro-pump is smaller than 500 mW [36].

Appendix A

Technical parameters of the piezoelectric materials, which are used in this study, presented in Table A1.

Table A1  
Technical parameter of the piezoelectric material.

Technical Parameter	Symbol	Unit	Data
Relative dielectric constant	$\epsilon_{r3}^T$	—	3500
Dielectric loss	$tg\delta$	%	2
Radial electromechanical coupling factor	$K_p$	—	0.65
Length electromechanical coupling factor	$K_{31}$	—	0.35
Vertical electromechanical coupling factor	$K_{33}$	—	0.70
Thickness vertical electromechanical coupling factor	$K_T$	—	0.55
Piezoelectric strain coefficient	$d_{31}$	$10^{-12}$ c/N	-280
Piezoelectric strain coefficient	$d_{33}$	$10^{-12}$ c/N	650
Piezoelectric voltage coefficient	$g_{31}$	$10^{-3}$ Vm/N	13
Piezoelectric voltage coefficient	$g_{33}$	$10^{-3}$ Vm/N	28
Compliance coefficient	$S_{11}^E$	$10^{-12}$ m <sup>2</sup> /N	16
Poisson's ratio	$\sigma^E$	—	0.36
Mechanical quality factor	$Q_m$	—	60
Maximum voltage	$V_{max}$	V	8
Maximum Current	$I_{max}$	A	5

## References

- [1] S. Ulukus, A. Yener, E. Erkip, O. Simeone, M. Zorzi, P. Grover, K. Huang, Energy harvesting wireless communications: a review of recent advances, *IEEE J. Selected Areas Commun.* 33 (3) (2015) 360–381.
- [2] A. Pop-Vadean, P. Pop, T. Latinovic, C. Barz, C. Lung, Harvesting Energy an Sustainable Power Source, Replace Batteries for Powering WSN and Devices on the IoT, p. 012043 (2018).
- [3] J. Lee, B. Choi, Development of a piezoelectric energy harvesting system for implementing wireless sensors on the tires, *Energy Convers. Manage.* 78 (2014) 32–38.
- [4] M. Febbo, S. Machado, C. Gatti, J. Ramirez, An out-of-plane rotational energy harvesting system for low frequency environments, *Energy Convers. Manage.* 152 (2017) 166–175.
- [5] A. Clément, P. McCullen, A. Falcão, A. Fiorentino, F. Gardner, K. Hammarlund, G. Lemonis, T. Lewis, K. Nielsen, S. Petroncini, Wave energy in Europe: current status and perspectives, *Renew. Sustain. Energy Rev.* 6 (5) (2002) 405–431.
- [6] António F. de O F, Wave energy utilization: a review of the technologies, *Renew. Sustain. Energy Rev.* 14 (3) (2010) 899–918 1.
- [7] I. López, J. Andreu, S. Ceballos, I.M. de Alegría, I. Kortabarria, Review of wave energy technologies and the necessary power-equipment, *Renew. Sustain. Energy Rev.* 27 (2013) 413–434.
- [8] R. Alamian, R. Shafaghat, S.J. Miri, N. Yazdanshenas, M. Shakeri, Evaluation of technologies for harvesting wave energy in Caspian Sea, *Renew. Sustain. Energy Rev.* 32 (2014) 468–476.
- [9] T. Whittaker, W. Beattie, M. Folley, C. Boake, A. Wright, M. Osterried, T. Heath, “The limpet wave power project—the first years of operation, *Renew. Energy* (2004).
- [10] M. Kramer, L. Marquis, P. Frigaard, Performance Evaluation of the Wavestar Prototype, EWTEC 2011 conference in Southampton, UK, 2011.
- [11] R. Henderson, Design, simulation, and testing of a novel hydraulic power take-off system for the Pelamis wave energy converter, *Renew. Energy* 31 (2) (2006) 271–283.
- [12] S. Priya, Advances in energy harvesting using low profile piezoelectric transducers, *J. Electroceram.* 19 (1) (2007) 167–184.
- [13] D.M. Dodge, *Illustrated History of Wind Power Development*, (2001) <http://telosnet.com/wind/early.html>.
- [14] A. Zurkinden, F. Campanile, L. Martinelli, *Wave Energy Converter Through Piezoelectric Polymers*, (2007).
- [15] R. Murray, J. Rastegar, Novel Two-stage Piezoelectric-based Ocean Wave Energy Harvesters for Moored or Unmoored Buoys, p. 72880E. (2009).
- [16] B. Orazov, O. O’Reilly, Ö. Savaş, On the dynamics of a novel ocean wave energy converter, *J. Sound Vib.* 329 (24) (2010) 5058–5069.
- [17] A. Erturk, G. Delporte, Underwater thrust and power generation using flexible piezoelectric composites: an experimental investigation toward self-powered swimmer-sensor platforms, *Smart Mater. Struct.* 20 (12) (2011) 125013.
- [18] Y. Cha, H. Kim, M. Porfiri, Energy harvesting from underwater base excitation of a piezoelectric composite beam, *Smart Mater. Struct.* 22 (11) (2013) 115026.
- [19] X. Xie, Q. Wang, N. Wu, Potential of a piezoelectric energy harvester from sea waves, *J. Sound Vib.* 333 (5) (2014) 1421–1429.
- [20] X. Xie, Q. Wang, N. Wu, Energy harvesting from transverse ocean waves by a piezoelectric plate, *Int. J. Eng. Sci.* 81 (2014) 41–48.
- [21] F. Cellini, J. Pounds, S.D. Peterson, M. Porfiri, Underwater energy harvesting from a turbine hosting ionic polymer metal composites, *Smart Mater. Struct.* 23 (8) (2014) 085023.
- [22] N. Wu, Q. Wang, X. Xie, Ocean wave energy harvesting with a piezoelectric coupled buoy structure, *Appl. Ocean Res.* 50 (2015) 110–118.
- [23] N. Viet, X. Xie, K. Liew, N. Banthia, Q. Wang, Energy harvesting from ocean waves by a floating energy harvester, *Energy* 112 (2016) 1219–1226.
- [24] W.S. Hwang, J.H. Ahn, S.Y. Jeong, H.J. Jung, S.K. Hong, J.Y. Choi, J.Y. Cho, J.H. Kim, T.H. Sung, Design of piezoelectric ocean-wave energy harvester using sway movement, *Sensor Actuat. A: Phys.* 260 (2017) 191–197.
- [25] H. Mutsuda, Y. Tanaka, R. Patel, Y. Doi, Y. Moriyama, Y. Umino, “A painting type of flexible piezoelectric device for ocean energy harvesting, *Appl. Ocean Res.* 68 (2017) 182–193.
- [26] R.W. Clough, J. Penzien, *Dynamics of Structures, Computers & Structures, Inc*, 2003.
- [27] A. Erturk, D.J. Inman, *Piezoelectric Energy Harvesting*, John Wiley & Sons, 2011.
- [28] A. Afsharfard, Application of nonlinear magnetic vibro-impact vibration suppressor and energy harvester, *Mech. Syst. Signal. Process.* 98 (2018) 371–381.
- [29] S.S. Rao, *Vibration of Continuous Systems*, John Wiley & Sons, 2007.
- [30] M.E. McCormick, *Ocean Engineering Mechanics: With Applications*, Cambridge University Press, 2009.
- [31] A. Khaligh, O.C. Onar, *Energy Harvesting: Solar, Wind, and Ocean Energy Conversion Systems*, CRC press, 2009.
- [32] P. Le Tirant, J. Meunier, *Anchoring of Floating Structures: Editions Technip*, (1990).
- [33] M. Eriksson, R. Waters, O. Svensson, J. Isberg, M. Leijon, Wave power absorption: experiments in open sea and simulation, *J. Appl. Phys.* 102 (8) (2007) 084910.
- [34] M. Stelzer, R. Joshi, Evaluation of wave energy generation from buoy heave response based on linear generator concepts, *J. Renew. Sustainable Energy* 4 (6) (2012) 063137.
- [35] <http://www.ndbc.noaa.gov/station/> Accessed 1 May 2018.
- [36] [http://www.process-valves.com/media/specs/Burkert\\_Type\\_7604\\_Micro\\_Pump\\_11mm/](http://www.process-valves.com/media/specs/Burkert_Type_7604_Micro_Pump_11mm/) Accessed 1 May 2018.
- [37] <https://www.aanderaa.com/> Accessed 1 May 2018.
- [38] <http://www.revrobotics.com/content/docs/REV-11-1107-DS/> Accessed 1 May 2018.
- [39] <http://www.stevenswater.com/resources/datasheets/dts-12datasheet/> Accessed 1 May 2018.
- [40] [https://www.ayyeka.com/img/kits/SE00017\\_Turbidity-and-Temperature-Sensor-Ponsel\\_NEPHELOMETRIC\\_Datasheet/](https://www.ayyeka.com/img/kits/SE00017_Turbidity-and-Temperature-Sensor-Ponsel_NEPHELOMETRIC_Datasheet/) Accessed 1 May 2018.
- [41] [https://www.ablicinc.com/en/doc/datasheet/temperature\\_sensor/S5851A\\_E/](https://www.ablicinc.com/en/doc/datasheet/temperature_sensor/S5851A_E/) Accessed 1 May 2018.
- [42] <http://gillinstruments.com/data/datasheets/windsonic/> Accessed 1 May 2018.